Supplementary Information

Multiscale Simulation of Eco-Friendly Perovskites under Space Radiation

Mustafa Kareem[1,2,*], Bassam Thaban[1], Asha Rajiv[3], Badri Narayan Sahu[4], Sridharan Sundharam[5], Prakhar Tomar[6]

[1]College of Remote Sensing and Geophysics, Al-Karkh University of Science, Al-Karkh Side, Haifa St. Hamada Palace, Baghdad 10011, Iraq
[2]College of Science, University of Warith Al-Anbiyaa, 56001 Karbala, Iraq
[3]Department of Physics & Electronics, School of Sciences, JAIN (Deemed to be University), Bangalore, Karnataka, India
[4]Department of Electronics & Communication Engineering, Siksha 'O' Anusandhan (Deemed to be University), Bhubaneswar, Odisha-751030, India
[5]Department of Physics, Sathyabama Institute of Science and Technology, Chennai, Tamil Nadu, India
[6]Centre for Research Impact & Outcome, Chitkara University Institute of Engineering and Technology, Chitkara University, Rajpura, 140401, Punjab, India

Corresponding author emails:
* dr.mustafa@kus.edu.iq

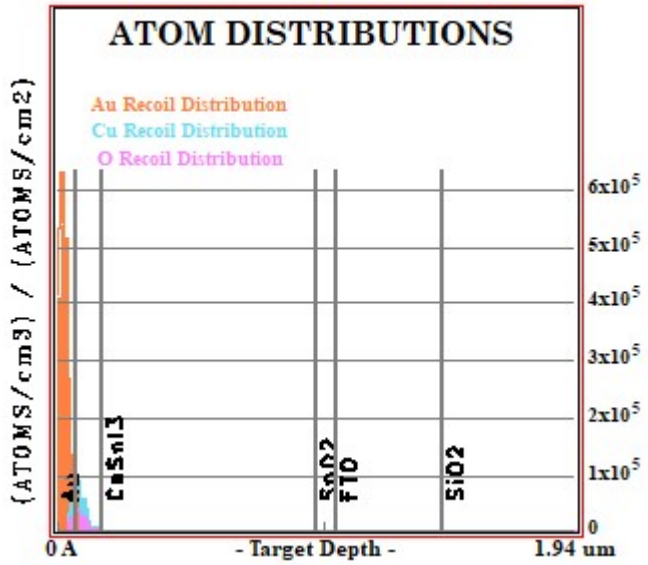

Figure S1: Element-Wise distribution of recoil atoms across the layers of $CsSnI_3$ device at an incident energy of 0.01 MeV.

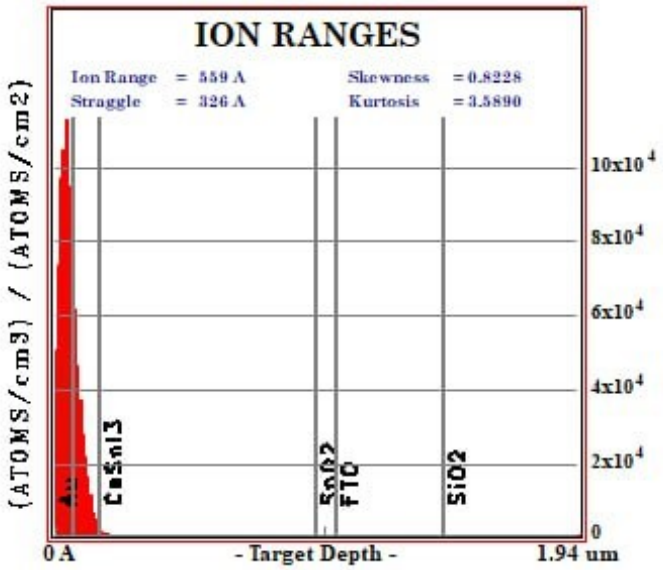

Figure S2: Ion distribution across the layers of $CsSnI_3$ device at an incident energy of 0.01 MeV.

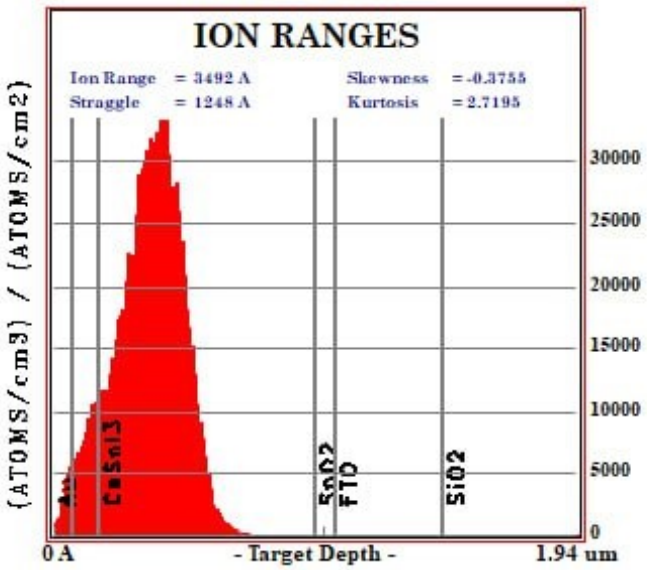

Figure S3: Ion distribution across the layers of $CsSnI_3$ device at an incident energy of 0.05 MeV.

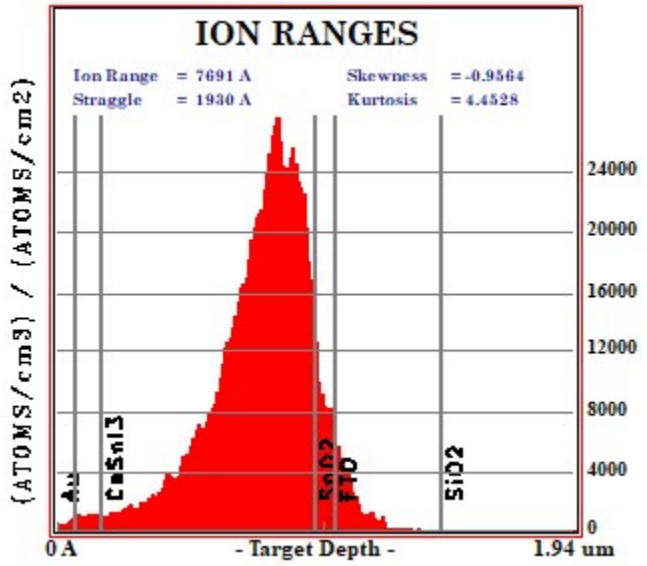

Figure S4: Ion distribution across the layers of $CsSnI_3$ device at an incident energy of 0.1 MeV.

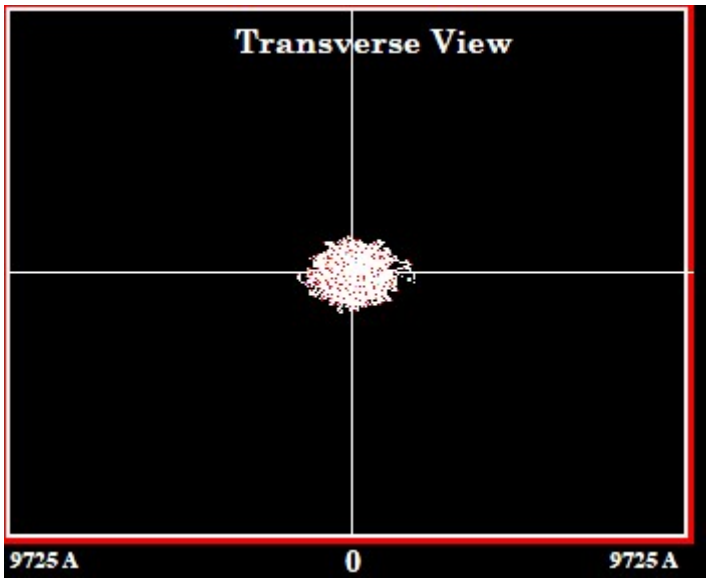

Figure S5: Proton trajectory in *xy*-plane for $CsSnI_3$ device at 0.01 MeV.

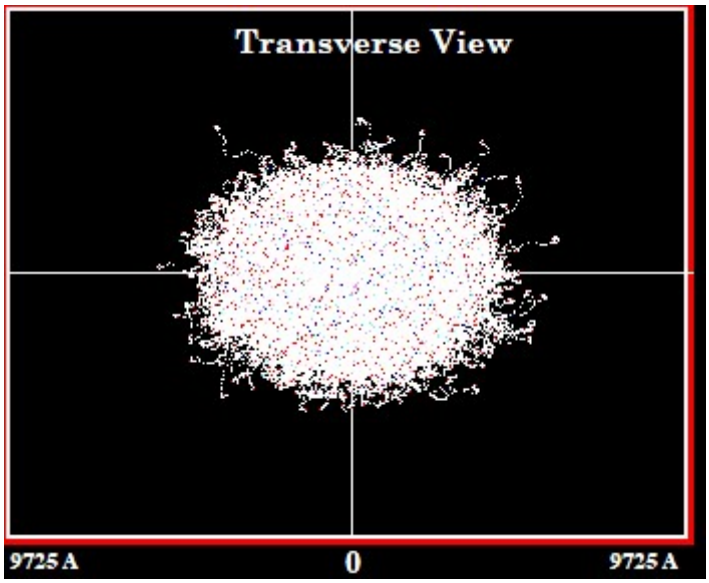

Figure S6: Proton trajectory in *xy*-plane for $CsSnI_3$ device at 0.05 MeV.

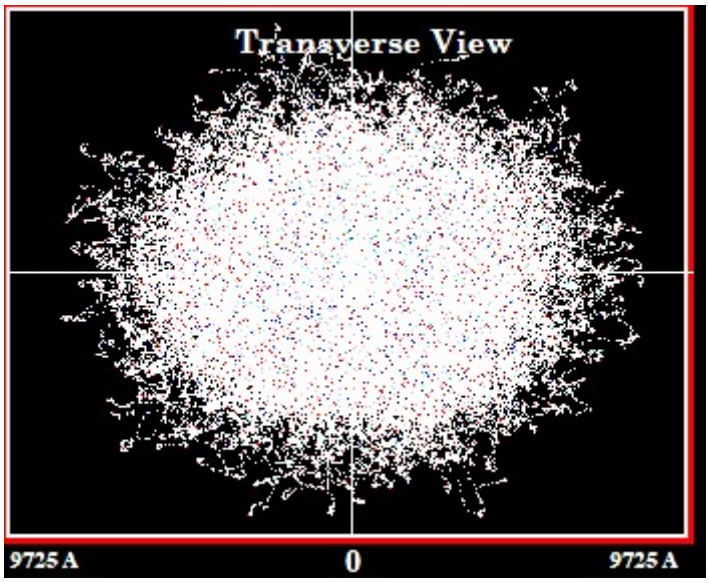

Figure S7: Proton trajectory in *xy*-plane for $CsSnI_3$ device at 0.1 MeV.

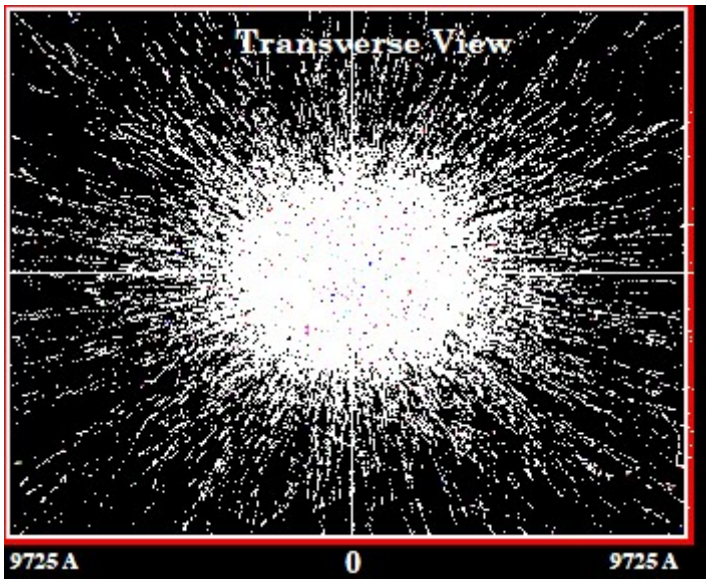

Figure S8: Proton trajectory in *xy*-plane for $CsSnI_3$ device at 0.3 MeV.

Figure S9: Proton trajectory in xy-plane for $CsSnI_3$ device at 0.5 MeV.

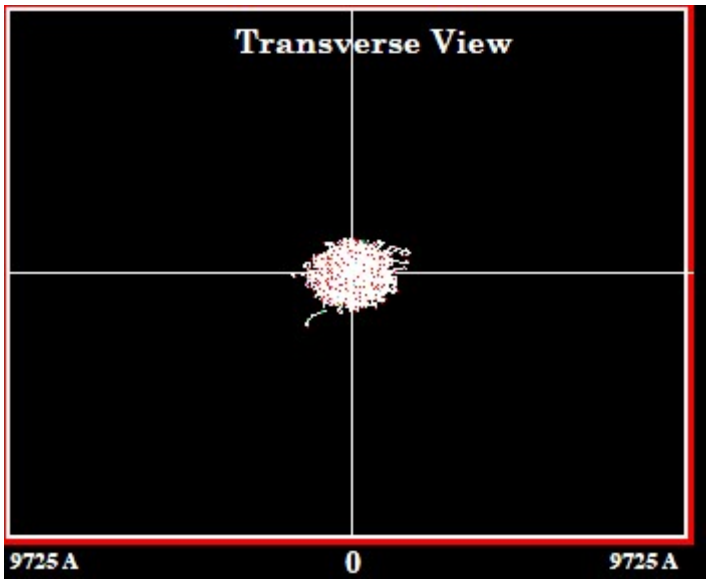

Figure S10: Proton trajectory in *xy*-plane for $MASnI_3$ device at 0.01 MeV.

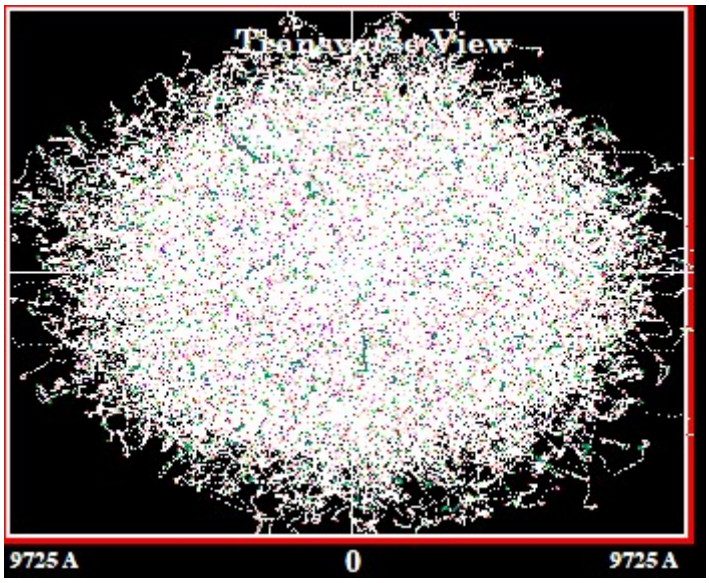

Figure S11: Proton trajectory in *xy*-plane for $MASnI_3$ device at 0.05 MeV

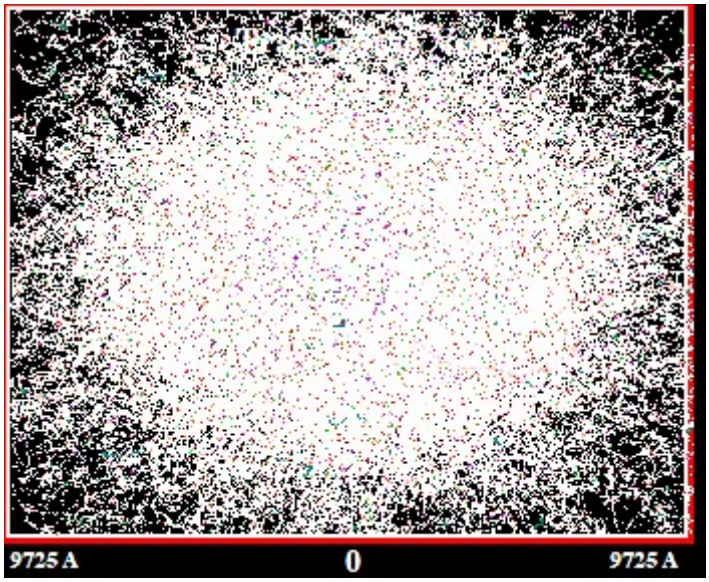

Figure S12: Proton trajectory in *xy*-plane for $MASnI_3$ device at 0.1 MeV.

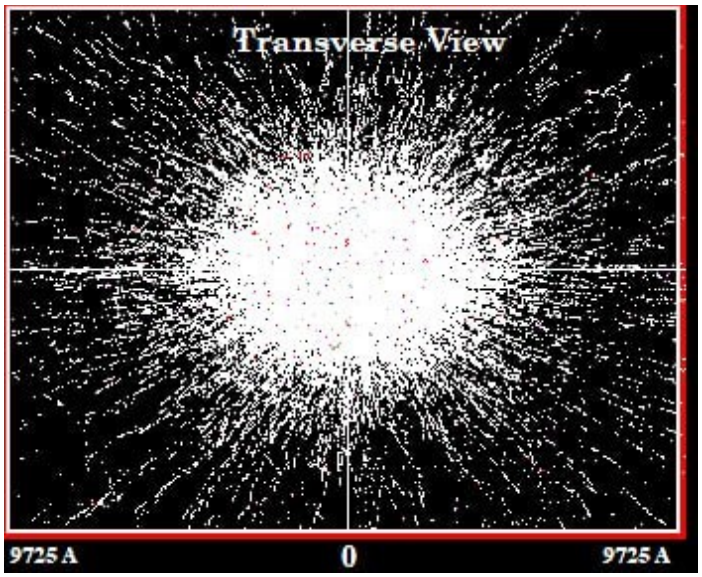

Figure S13: Proton trajectory in *xy*-plane for $MASnI_3$ device at 0.3 MeV.

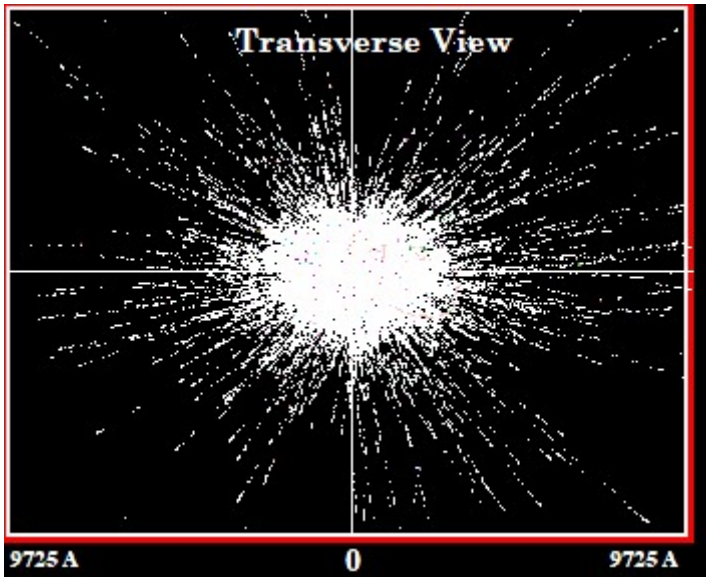

Figure S14: Proton trajectory in *xy*-plane for $MASnI_3$ device at 0.5 MeV.

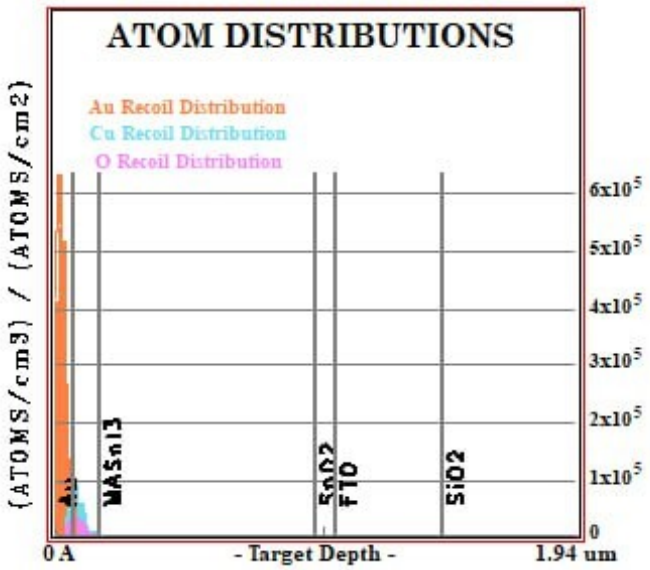

Figure S15: Element-Wise distribution of recoil atoms across the layers of $MASnI_3$ device at an incident energy of 0.01 MeV.

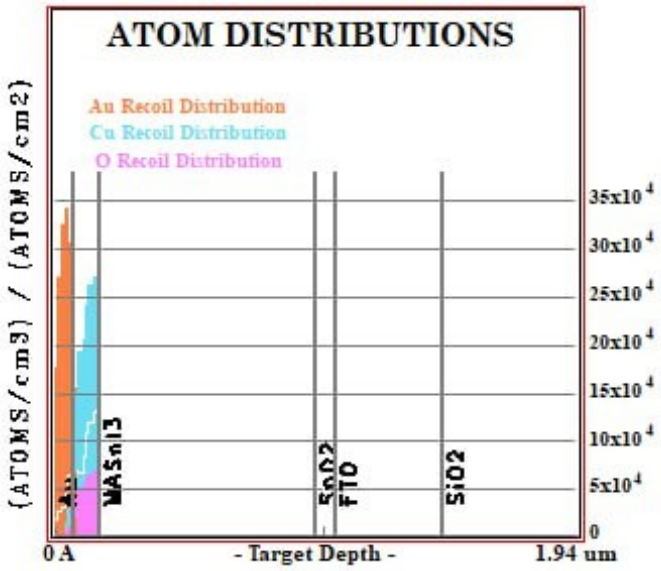

Figure S16: Element-Wise distribution of recoil atoms across the layers of $MASnI_3$ at an incident energy of 0.05 MeV.

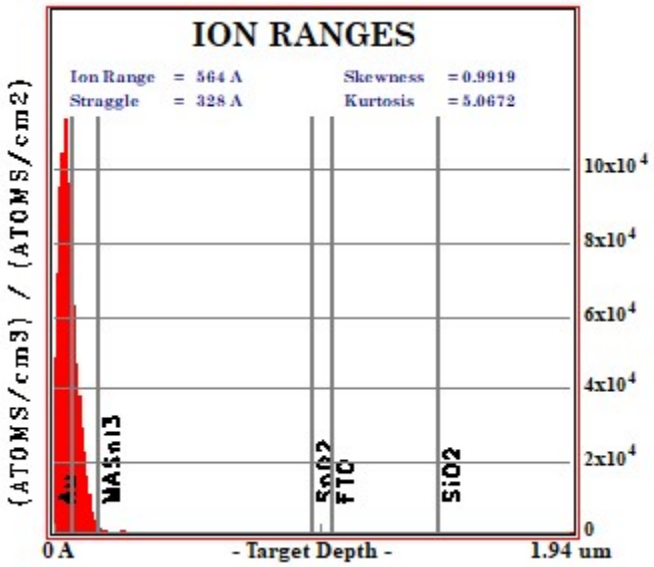

Figure S17: Ion distribution across the layers of $MASnI_3$ device at an incident energy of 0.01 MeV.

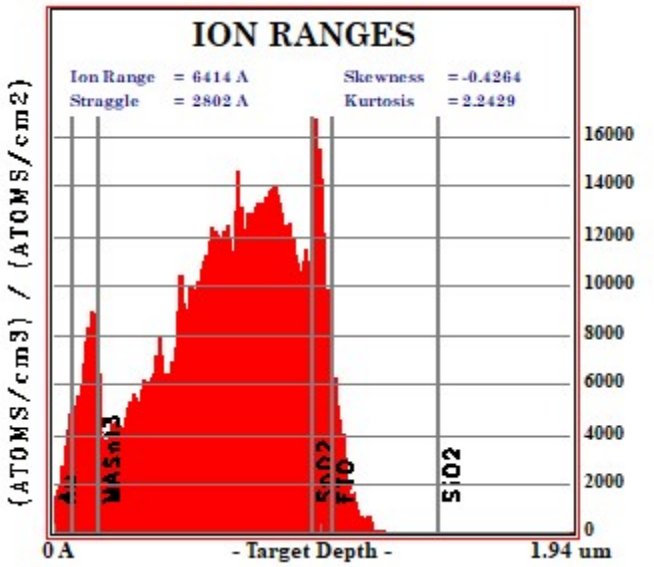

Figure S18: Ion distribution across the layers of $MASnI_3$ device at an incident energy of 0.05 MeV.

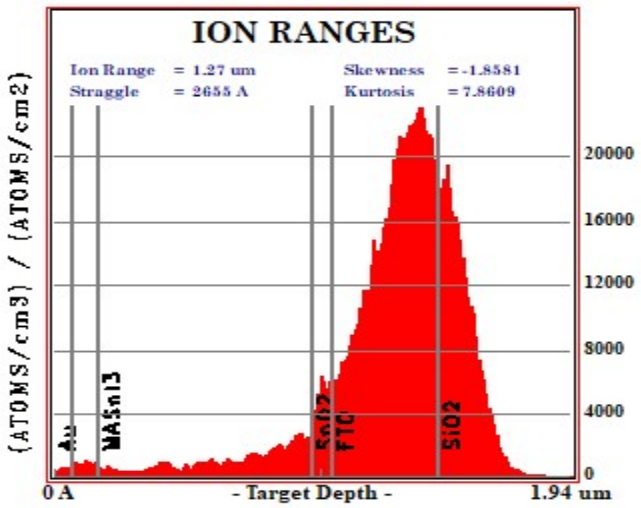

Figure S19: Ion distribution across the layers of $MASnI_3$ device at an incident energy of 0.1 MeV.

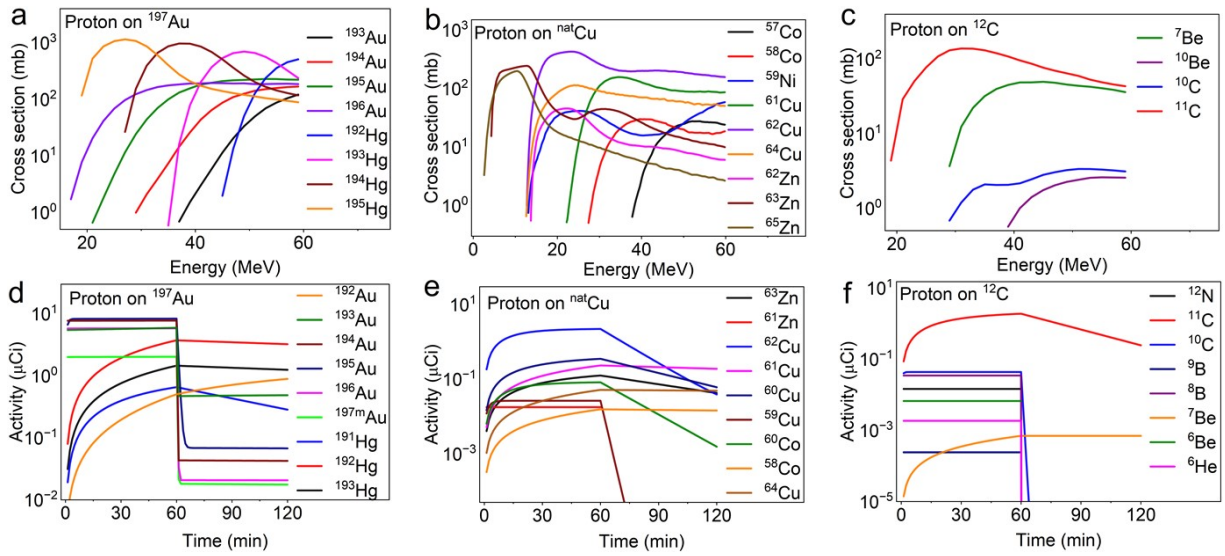

Figure S20: Analysis of proton-matter interactions using the TALYS nuclear reaction code. Simulated proton-induced reaction cross sections for **(a)** ^{197}Au, **(b)** ^{nat}Cu, and **(c)** ^{12}C target isotopes as a function of incident proton energy (0–60 MeV). The corresponding time-dependent radioactivity (up to 25 hours) of **(d)** ^{197}Au, **(e)** ^{nat}Cu, and **(f)** ^{12}C reaction products.

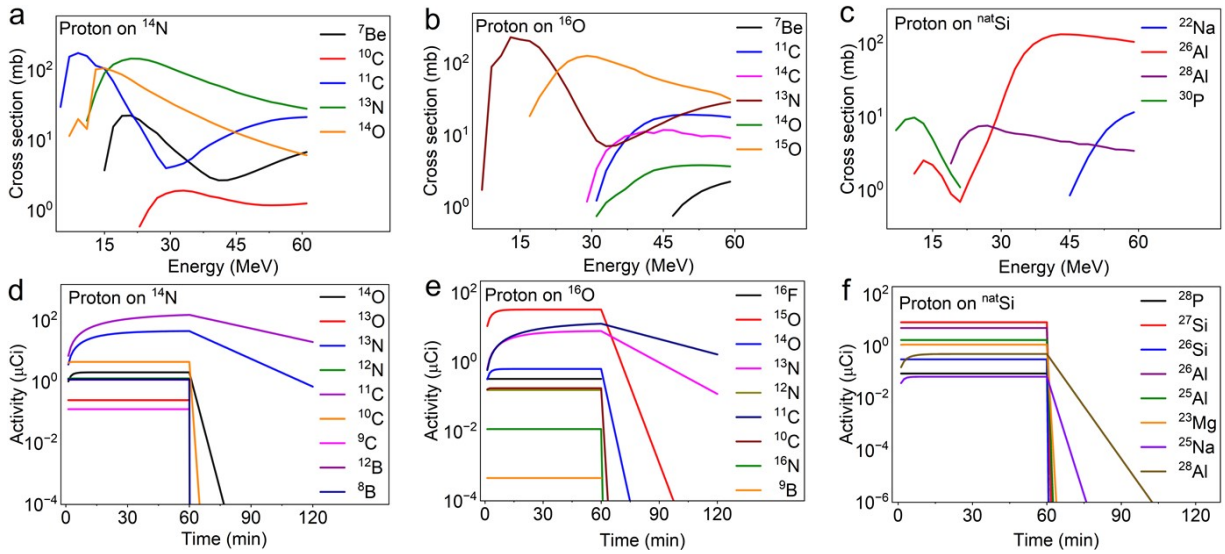

Figure S21: Analysis of proton-matter interactions using the TALYS nuclear reaction code. Simulated proton-induced reaction cross sections for **(a)** ^{14}N, **(b)** ^{16}O, and **(c)** ^{nat}Si target isotopes as a function of incident proton energy (0-60 MeV). The corresponding time-dependent radioactivity (up to 25 hours) of **(d)** ^{14}N, **(e)** ^{16}O, and **(f)** ^{nat}Si reaction products.

Note1:

A good overall agreement between the TALYS predicted excitation functions and the experimental cross section data available in the EXFOR database for the selected benchmark reactions. For ^{nat}Sn(p,x)^{117}Sb, the corresponding EXFOR datasets are provided as the reference set [1-3]. For ^{133}Cs(p,3n)^{131}Ba, the EXFOR datasets are listed in [4-8]. For ^{127}I(p,3n)^{125}Xe, the EXFOR datasets are compiled in [9-15]. For ^{nat}Cu(p,x)^{63}Zn, the associated EXFOR datasets are given in [16-27]. The TALYS simulations capture the main experimental features, including the reaction onset, the overall energy dependent behavior, and the approximate locations and magnitudes of the cross-section maxima. Minor discrepancies at the highest energies for some channels can be attributed to the expected limitations of global nuclear reaction modeling and to variations among experimental datasets. Overall, this benchmark comparison supports the reliability of the adopted TALYS settings and increases confidence in the calculated cross sections and activation estimates reported for the remaining reactions considered in this Supplementary Information.

Table S1. Interface parameters of SnO_2/Perovskite/Cu_2O structure.

Parameters/Interfaces	$SnO_2/CsSnI_3$	$CsSnI_3/Cu_2O$	$SnO_2/MASnI_3$	$MASnI_3/Cu_2O$
Defect type	Neutral	Neutral	Neutral	Neutral
Capture cross section for electrons (cm^2)	1×10^{-19}	1×10^{-19}	1×10^{-19}	1×10^{-19}
Capture cross section for holes (cm^2)	1×10^{-19}	1×10^{-19}	1×10^{-19}	1×10^{-19}
Energetic Distribution	Single	single	single	single
Reference for defect energy level E_t	Above the highest E_V	Above the highest E_V	Above the highest E_V	Above the highest E_V
Energy with respect to reference (eV)	0.600	0.600	0.600	0.600
Total density ($1/cm^2$)	1×10^{10}	1×10^{10}	1×10^{10}	1×10^{10}

Table S2: Comparison of photovoltaic parameters for simulated $CsSnI_3$ and $MASnI_3$ PSCs.

Device	V_{OC} (V)	J_{SC} (mA/cm^2)	FF (%)	PCE (%)
$CsSnI_3$ PSC	0.758	37.25	67.64	14.05
$MAPSnI_3$ PSC	0.821	40.22	71.71	17.41

Table S3: Summary of proton-induced nuclear reactions on different elements calculated using TALYS.

Target	Natural Abundance (%)	Nuclide	Reaction Channel	Threshold Energy (MeV)	Max. Cross Section (mb)
^{97}Au	100	^{193}Au	(p,2n+t)	21.64	174.89
		^{194}Au	(p,n+t)	14.73	181.43
		^{195}Au	(p,t)	6.26	229.99
		^{196}Au	(p,d)	5.87	193.69
		^{192}Hg	(p,6n)	40.47	516.89
		^{193}Hg	(p,5n)	33.31	696.47
		^{194}Hg	(p,4n)	24.07	968.09
		^{195}Hg	(p,3n)	17.13	1146.23
		^{196}Hg	(p,2n)	8.21	982.27
^{nat}Cu	^{63}Cu: 69.17 ^{65}Cu: 30.83	^{60}Ni	(p,x)	Non	151.27
		^{61}Ni			154.95
		^{61}Cu			156.90
		^{62}Cu			427.33
		^{63}Zn			243.97
		^{64}Zn			161.18
		^{65}Zn			199.00
^{133}Cs	100	^{129}Cs	(p,2n+t)	24.56	157.09
		^{130}Cs	(p,n+t)	17.03	164.72
		^{131}Cs	(p,t)	77.34	235.12
		^{132}Cs	(p,d)	6.82	227.49
		^{128}Ba	(p,6n)	44.17	225.34
		^{129}Ba	(p,5n)	36.35	375.88
		^{130}Ba	(p,4n)	26.00	658.46
		^{131}Ba	(p,3n)	18.45	928.86
		^{132}Ba	(p,2n)	8.55	963.34
		^{133}Ba	(p,n)	1.31	360.82
^{nat}Sn	^{112}Sn: 0.97 ^{114}Sn: 0.66 ^{115}Sn: 0.34 ^{116}Sn: 14.54 ^{117}Sn: 7.68 ^{118}Sn: 24.22 ^{119}Sn: 8.59 ^{120}Sn: 32.58 ^{122}Sn: 4.63 ^{124}Sn: 5.79	^{113}Sn	(p,x)	Non	95.31
		^{114}Sb			65.13
		^{115}Sb			144.32
		^{116}Sb			147.82
		^{117}Sb			297.70
		^{118}Sb			323.38
		^{119}Sb			376.99
		^{120}Sb			58.22
		^{123}Sb			63.66

^{127}I	100	^{123}I	(p,2n+t)	25.05	149.57
		^{124}I	(p,n+t)	17.48	169.66
		^{125}I	(p,t)	7.87	231.76
		^{126}I	(p,d)	6.97	233.58
		^{122}Xe	(p,6n)	45.12	160.02
		^{123}Xe	(p,5n)	37.09	298.11
		^{124}Xe	(p,4n)	26.52	567.37
		^{125}Xe	(p,3n)	18.85	876.77
		^{126}Xe	(p,2n)	8.75	997.81
		^{127}Xe	(p,n)	1.45	381.42
^{12}C	99	^{6}Li	(p,^{3}He+a)	26.18	48.01
		^{7}Li	(p,2p+a)	26.68	28.12
		^{7}Be	(p,d+a)	26.06	50.19
		^{8}Be	(p,p+a)	7.98	103.47
		^{9}Be	(p,p+^{3}He)	28.48	11.88
		^{9}B	(p,a)	8.18	261.42
		^{10}B	(p,^{3}He)	21.34	52.26
		^{11}B	(p,2p)	17.29	96.62
		^{11}C	(p,d)	17.88	140.35
		^{12}N	(p,n)	19.64	36.35
^{14}N	99.6	^{8}Be	(p, ^{3}He + a)	13.02	88.11
		^{9}B	(p, d + a)	19.10	28.77
		^{10}B	(p, p + a)	12.44	53.64
		^{11}B	(p, p + ^{3}He)	22.22	27.11
		^{11}C	(p,a)	3.13	177.74
		^{12}C	(p, ^{3}He)	5.11	188.44
		^{13}C	(p,2p)	8.09	154.29
		^{13}N	(p,d)	8.92	148.04
		^{14}O	(p,n)	6.35	108.06
^{16}O	99.76	^{8}Be	(p,2a)	15.44	33.36
		^{11}B	(p,2p + a)	24.57	15.78
		^{11}C	(p,d + a)	25.14	14.93
		^{12}C	(p,p + a)	7.61	246.14
		^{13}C	(p, p + ^{3}He)	24.23	56.45
		^{13}N	(p,a)	5.56	231.83
		^{14}N	(p, ^{3}He)	16.20	162.62
		^{15}N	(p,2p)	12.89	128.34
		^{15}O	(p,d)	14.28	123.38
		^{16}F	(p,n)	17.21	18.56
^{nat}Si	^{28}Si: 92.23 ^{29}Si: 4.68 ^{30}Si: 3.08	^{23}Na	(p,x)	Non	35.76
		^{24}Mg			147.76
		^{25}Mg			94.35
		^{26}Mg			90.61
		^{25}Al			54.34
		^{26}Al			135.15
		^{27}Al			376.63
		^{27}Si			126.79

Reference

[1] M.U. Khandaker, K. Kim, K.-S. Kim, M. Lee, Y.S. Lee, G. Kim, Y.-S. Cho, Y.-O. Lee, Excitation functions of the proton-induced nuclear reactions on natSn up to 40 MeV, Nuclear Instruments and Methods in Physics Research Section B: Beam Interactions with Materials and Atoms 267 (2009) 23–31. https://doi.org/10.1016/j.nimb.2008.11.017.

[2] A. Hermanne, F. Tárkányi, F. Ditrói, S. Takács, R. Adam Rebeles, M.S. Uddin, M. Hagiwara, M. Baba, Yu. Shubin, S.F. Kovalev, Experimental study of the excitation functions of proton induced reactions on natSn up to 65 MeV, Nuclear Instruments and Methods in Physics Research Section B: Beam Interactions with Materials and Atoms 247 (2006) 180–191. https://doi.org/10.1016/j.nimb.2006.02.005.

[3] S.M. Kormali, D.L. Swindle, E.A. Schweikert, Charged particle activation of medium Z elements, J. Radioanal. Chem. 31 (1976) 437–450. https://doi.org/10.1007/BF02518508.

[4] F. Tárkányi, A. Hermanne, S. Takács, F. Ditrói, B. Király, H. Yamazaki, M. Baba, A. Mohammadi, A.V. Ignatyuk, New measurements and evaluation of excitation functions for (p,xn), (p,pxn) and (p,2pxn) reactions on 133Cs up to 70 MeV proton energy, Applied Radiation and Isotopes 68 (2010) 47–58. https://doi.org/10.1016/j.apradiso.2009.09.069.

[5] E. Porras, F. Sánchez, V. Reglero, B. Cordier, A.J. Dean, F. Lei, J.M. Pérez, B.M. Swinyard, Production rate of proton-induced isotopes in different materials, Nuclear Instruments and Methods in Physics Research Section B: Beam Interactions with Materials and Atoms 160 (2000) 73–125. https://doi.org/10.1016/S0168-583X(99)00556-X.

[6] K. Sakamoto, M. Dohniwa, K. Okada, Excitation functions for (p,xn) and (p,pxn) reactions on natural 79 + 81Br, 85 + 87Rb, 127I and 133Cs upto *E*p=52 MeV, The International Journal of Applied Radiation and Isotopes 36 (1985) 481–488. https://doi.org/10.1016/0020-708X(85)90213-3.

[7] M.C. Lagunas-Solar, F.E. Little, H.A. Moore, Cyclotron production of 128Cs (3.62 min). A new positron-emitting radionuclide for medical applications, The International Journal of Applied Radiation and Isotopes 33 (1982) 619–628. https://doi.org/10.1016/0020-708X(82)90059-X.

[8] R.W. Fink, E.O. Wiig, Reactions of Cesium with Protons at 60, 80, 100, 150, and 240 Mev, Phys. Rev. 96 (1954) 185–187. https://doi.org/10.1103/PhysRev.96.185.

[9] M.C. Lagunas-Solar, O.F. Carvacho, L.J. Harris, C.A. Mathis, Cyclotron production of 122Xe(20.1 h)→122I (β + 77%; EC 23%; 3.6 min) for positron emission tomography. Current methods and potential developments, International Journal of Radiation Applications and Instrumentation. Part A. Applied Radiation and Isotopes 37 (1986) 835–842. https://doi.org/10.1016/0883-2889(86)90279-0.

[10] K. Suzuki, Production of Pure 123I by the 127I (p, 5n) 123Xe→123I Reaction, Radioisotopes 35 (1986) 235–241. https://doi.org/10.3769/radioisotopes.35.5_235.

[11] K. Sakamoto, M. Dohniwa, K. Okada, Excitation functions for (p,xn) and (p,pxn) reactions on natural 79 + 81Br, 85 + 87Rb, 127I and 133Cs upto Ep=52 MeV, The International Journal of Applied Radiation and Isotopes 36 (1985) 481–488. https://doi.org/10.1016/0020-708X(85)90213-3.

[12] D.B. Syme, E. Wood, I.M. Blair, S. Kew, M. Perry, P. Cooper, Yield curves for cyclotron production of 123I, 125I and 121I by 127I (p,xn) Xe → (β) → I reactions, The International Journal of Applied Radiation and Isotopes 29 (1978) 29–38. https://doi.org/10.1016/0020-708X(78)90154-0.

[13] H. Lundqvist, P. Malmborg, B. Långström, Suparb na Chiengmai, Simple production of 77Br− and 123I− and their use in the labelling of [77Br]BrUdR and [123I]IUdR, The International Journal of Applied Radiation and Isotopes 30 (1979) 39–43. https://doi.org/10.1016/0020-708X(79)90095-4.

[14] A.M.J. Paans, W. Vaalburg, G. van Herk, M.G. Woldring, Excitation function for the production of 123I via the 127I(p, 5n) 123Xe reaction, The International Journal of Applied Radiation and Isotopes 27 (1976) 465–467. https://doi.org/10.1016/0020-708X(76)90068-5.

[15] S.R. Wilkins, S.T. Shimore, H.H. Hines, J.A. Jungerman, F. Hegedus, G.L. DeNardo, Excitation functions and yields for 123I production using the 127I(<p, 5n) 123Xe reaction, The International Journal of Applied Radiation and Isotopes 26 (1975) 279–283. https://doi.org/10.1016/0020-708X(75)90162-3.

[16] N. Muhammad, M. Adil, S.U. Mulk, I. Ahmad, J. Hussain, T.A. Abbas, M. Anwer, A. Makinaga, M. Shahid, Proton and alpha-particle activation studies of natFe, natCu, natTi and natW targets at low energies, Radiochimica Acta 113 (2025) 9–21. https://doi.org/10.1515/ract-2024-0310.

[17] M. Anwer, A. Naz, I. Ahmad, M. Usman, J. Hussain, S.Z. Ilyas, M. Shahid, Ion beam activation of natCu, natTi, natNi and measurement of product formation cross sections at low energy (<10 MeV), Radiochimica Acta 110 (2022) 799–808. https://doi.org/10.1515/ract-2021-1132.

[18] M.B. Fox, A.S. Voyles, J.T. Morrell, L.A. Bernstein, J.C. Batchelder, E.R. Birnbaum, C.S. Cutler, A.J. Koning, A.M. Lewis, D.G. Medvedev, F.M. Nortier, E.M. O'Brien, C. Vermeulen, Measurement and modeling of proton-induced reactions on arsenic from 35 to 200 MeV, Phys. Rev. C 104 (2021) 064615. https://doi.org/10.1103/PhysRevC.104.064615.

[19] J. Červenák, O. Lebeda, New cross-section data for proton-induced reactions on natTi and natCu with special regard to the beam monitoring, Nuclear Instruments and Methods in Physics Research Section B: Beam Interactions with Materials and Atoms 480 (2020) 78–97. https://doi.org/10.1016/j.nimb.2020.08.006.

[20] T. Siiskonen, J. Huikari, T. Haavisto, J. Bergman, S.-J. Heselius, J.-O. Lill, T. Lönnroth, K. Peräjärvi, Excitation functions of proton-induced reactions in natCu in the energy range 7–17 MeV, Applied Radiation and Isotopes 67 (2009) 2037–2039. https://doi.org/10.1016/j.apradiso.2008.11.005.

[21] F.S. Al-Saleh, A.A. Al-Harbi, A. Azzam, Excitation functions of proton induced nuclear reactions on natural copper using a medium-sized cyclotron, Radiochimica Acta 94 (2006) 391–396. https://doi.org/10.1524/ract.2006.94.8.391.

[22] S. Takács, F. Tárkányi, M. Sonck, A. Hermanne, New cross-sections and intercomparison of proton monitor reactions on Ti, Ni and Cu, Nuclear Instruments and Methods in Physics Research Section B: Beam Interactions with Materials and Atoms 188 (2002) 106–111. https://doi.org/10.1016/S0168-583X(01)01032-1.

[23] F. Szelecsényi, F. Tárkányi, S. Takács, A. Hermanne, M. Sonck, Y. Shubin, M.G. Mustafa, Z. Youxiang, Excitation function for the natTi(p,x)48V nuclear process: Evaluation and new measurements for practical applications, Nuclear Instruments and Methods in Physics Research Section B: Beam Interactions with Materials and Atoms 174 (2001) 47–64. https://doi.org/10.1016/S0168-583X(00)00516-4.

[24] S.J. Mills, G.F. Steyn, F.M. Nortier, Experimental and theoretical excitation functions of radionuclides produced in proton bombardment of copper up to 200 MeV, International Journal of Radiation Applications and Instrumentation. Part A. Applied Radiation and Isotopes 43 (1992) 1019–1030. https://doi.org/10.1016/0883-2889(92)90221-Y.

[25] V.N. Aleksandrov, M.P. Semenova, V.G. Semenov, Production cross section of radionuclides in (p, x) reactions at copper and nickel nuclei, At Energy 62 (1987) 478–481. https://doi.org/10.1007/BF01124118.

[26] A. Grütter, Excitation functions for radioactive isotopes produced by proton bombardment of Cu and Al in the energy range of 16 to 70 MeV, Nuclear Physics A 383 (1982) 98–108. https://doi.org/10.1016/0375-9474(82)90078-1.

[27] Y. Yoshizawa, H. Noma, T. Horiguchi, T. Katoh, S. Amemiya, M. Itoh, K. Hisatake, M. Sekikawa, K. Chida, Isotope separator on-line at INS FM cyclotron, Nuclear Instruments and Methods 134 (1976) 93–100. https://doi.org/10.1016/0029-554X(76)90128-2.